An analytical model for the thermal conductivity of silicon nanostructures

P. Chantrenne[a)]
Centre de Thermique de Lyon, Institut National des Sciences Appliquées, bâtiment Sadi Carnot, 20, Avenue A. Einstein, 69621 Villeurbanne Cedex, France

J. L. Barrat and X. Blase
Laboratoire de Physique de la Matière Condensée et Nanostructures, Université Claude Bernard Lyon 1 and Centre National de la Recherche Scientifique (CNRS), Batiment Léon Brillouin, 43 Boulevard du 11 Novembre, 69622 Villeurbanne Cedex, France

J. D. Gale
Nanochemistry Research Institute, Department of Applied Chemistry, Curtin University of Technology, P.O. Box U1987, Perth 6845, Western Australia

(Received 20 July 2004; accepted 7 March 2005; published online 6 May 2005)

A simple model of thermal conductivity, based on the harmonic theory of solids, is used to study the heat transfer in nanostructures. The thermal conductivity is obtained by summing the contribution of all the vibration modes of the system. All the vibrational properties (dispersion curves and relaxation time) that are used in the model are obtained using the data for bulk samples. The size effect is taken into account through the sampling of the Brillouin zone and the distance that a wave vector can travel between two boundaries in the structure. The model is used to predict the thermal conductivity of silicon nanowires and nanofilms, and demonstrates a good agreement with experimental results. Finally, using this model, the quality of the silicon interatomic potential, used for molecular-dynamics simulations of heat transfer, is evaluated. © *2005 American Institute of Physics*. [DOI: 10.1063/1.1898437]

I. INTRODUCTION

The thermal characterization of nanostructures and nanostructured materials is a fundamental issue for the reliability of the systems as microelectronic, microelectromechanical systems, energy conversion systems using the thermoelectric effect, lab on a chip, and super insulators. The thermal conductivity of such structures can either be measured or predicted. The measurement of the thermal conductivity is quite common for bulk materials, much less so for nanostructured materials, and remains a challenge that has been met only for a few nanostructures. Theoretical analysis and numerical simulations, on the other hand, readily provide information regarding heat transfer phenomena at the nanoscales. They can, in principle, accurately predict the thermal conductivity of nanostructures that have not already been produced or that are difficult to characterize experimentally. However, before entering such a predictive stage, it is necessary to check the validity of the results with experimental data.

In this context, silicon appears as one of the most interesting materials, since it is widely used for designing microelectronic devices. Moreover silicon crystals of different shapes have been produced with characteristic lengths ranging from some nanometer to centimeter. The thermal conductivity of bulk silicon has been measured over a large temperature range since the 1960s.[1–3] Silicon-based superlattices, nanofilms, nanowires, and nanoporous silicon have also been characterized experimentally.[4–8] If the electronic concentration is small enough, which is the case for intrinsic and moderately doped silicon, the heat transfer due to electrons is negligible compared to phonon heat transfer. Finally, the experimental conditions of the thermal-conductivity measurement of silicon nanostructures are such that radiative heat transfer is neglected toward phonon heat transfer. For all these reasons, silicon is a material that can be used as a benchmark for simple models such as the one discussed in this paper.

Models allowing an analytical calculation of the (phonon-dominated) thermal conductivity are, in general, based on the use of the standard kinetic theory within the relaxation-time approximation. They require the knowledge of the phonon properties: dispersion curves or density of states, group velocities, and relaxation time.[7,9–16] For simple models, a constant group velocity and a unique relaxation time may be considered for all the vibration modes (transverse and longitudinal), while for more complex models, the group velocity is calculated from the dispersion curves and the relaxation time may depend on the polarization. The temperature variations of the relaxation time depend on two phenomena: the variation of phonon density with the temperature (given by the Planck distribution function) and the variation of the anharmonicity with the temperature level. Several analytical expressions were proposed for the relaxation time, in which the parameters are determined in order to fit the experimental temperature dependence of the thermal conductivity. In these models, the phonon frequency ranges from 0 to a maximum value, which means that their wavelength ranges from infinity to a minimum value. For each system, it has to be checked that the energy contribution of the phonons with wavelength larger than the system size (which cannot exist in the system but are still considered in these models) is negligible towards the energy contribution

[a)]Electronic mail: patrice.chantrenne@insa-lyon.fr

of the other phonons. Qualitatively, for small systems at low temperatures, this condition might not be verified and the thermal conductivity might be overestimated. For silicon, models have been proposed to predict the thermal conductivity of bulk material, nanofilms, and nanowires.[7,9,12,15,16]

As the characteristic size of the nanostructures decreases, the influence of the boundary surfaces becomes more and more important. This can lead to significant modification of the vibrational properties (dispersion curves and/or the relaxation time) of the matter compared to the bulk properties. One way to take this effect into account is to use atomic scale simulations, in particular, classical molecular dynamics (MD).[17,18] The merit of this approach is that it explicitly allows for anharmonic effects, though conversely it neglects the quantization of the phonons, which is important at low temperatures. In MD simulations, the system is classical; i.e., the mean number of phonons does not depend on their vibration frequency. Consequently, the use of MD to study heat transfer is limited to high temperatures.

Due to the computational cost of MD, the accessible time scale is typically limited to the nanoscale. The maximum size that can be handled depends on the material and the shape of the nanostructure, but is always much less than 1 μm.

In MD simulations, the vibrational properties depend on the interatomic potential used to calculate the forces on the atoms. Their variations with temperature level and system size (especially for small system) are automatically taken into account. The quality of the interatomic potential is then a key issue for the reliability of the MD results. For silicon, several interatomic potentials have been proposed in the literature.[19] However, the only one that was used in MD simulations in order to determine its thermal conductivity[20–22] is the Stillinger–Weber (SW) potential.[23] It is argued that the SW model allows us to accurately simulate the melting temperature, the elastic constant tensor, the dispersion curves, and the thermal-expansion coefficient of bulk silicon. Comparing four interatomic potentials (SW,[23] Tersoff,[24] Harrison,[25] and Biswas and Hamann[26]), Cooley[27] concluded that the use of any of these models to calculate quantities with a significant vibrational contribution should proceed with caution. This comparison was based on the calculation of the elastic constants and two particular vibration frequencies. The computation of the thermal properties proposed in this work provides a different, more global, benchmark of interatomic potentials.

This paper is organized in three parts. In the Sec. II, a simple, semianalytical model is presented and the contribution of each vibration mode to the thermal conductivity is evaluated. In the Sec. III, this approach is used to predict the thermal conductivity of nanowires and nanofilms of different sections or thicknesses in order to compare with the existing experimental values. The same model, based on the vibrational properties and relaxation time of the bulk crystal, is used in all cases. The difference lies in the sampling of the vibrational modes in the first Brillouin zone, which becomes nonisotropic. Finally, the model is used to check the validity of the SW interatomic potential for MD simulations of heat transfer in silicon, and to determine the temperature above which the MD results are expected to be reliable.

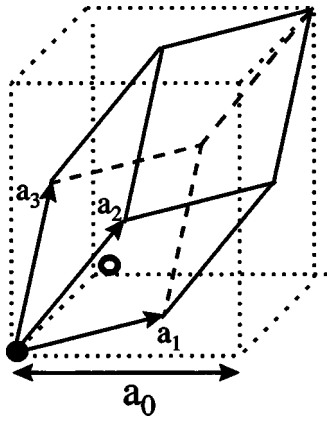

FIG. 1. The primitive unit cell of diamond containing two atoms.

II. MODEL FOR THE THERMAL CONDUCTIVITY

Using the elementary kinetic theory, the thermal conductivity λ in the direction z associated with the phonons (K,p) can be written as[28,29]

$$\lambda_z(K,p) = C(K,p)v^2(K,p)\tau(K,p)\cos^2[\theta_z(K)], \tag{1}$$

where K is the wave vector, p its polarization, and v the group velocity determined from the dispersion curves:

$$v(K,p) = d\omega(K,p)/dK, \tag{2}$$

with ω the angular velocity, $\tau(K,p)$ is the phonon relaxation time due to the phonon-scattering phenomena, $\theta_z(K)$ is the angle between the wave vector K and the direction z, and $C(K,p)$ is the specific heat per unit volume. It is the temperature derivative of the internal energy$U(K,p)$. For a system of volume V,[28]

$$C(K,p) = k_b x^2 \frac{e^x}{V(e^x-1)^2}, \tag{3}$$

$$x = \frac{\hbar\omega(K,p)}{k_b T}. \tag{4}$$

The total thermal conductivity and specific heat are the sum of the individual contributions due to all the wave vectors K and polarizations p:

$$\lambda_z = \sum_k \sum_p \lambda_z(K,p) = \sum_k \sum_p C(K,p)v^2(K,p)\tau(K,p)\cos^2[\theta_z(K)], \tag{5}$$

$$C = \sum_K \sum_p C(K,p). \tag{6}$$

Only the dispersion (for both optical and acoustic branches) curves are required to calculate the specific heat of the bulk crystal. The sampling of the wave vectors depends on the crystal shape.

For silicon, the crystal is composed of fcc elementary cells containing two atoms (Fig. 1). Thus there are six polar-

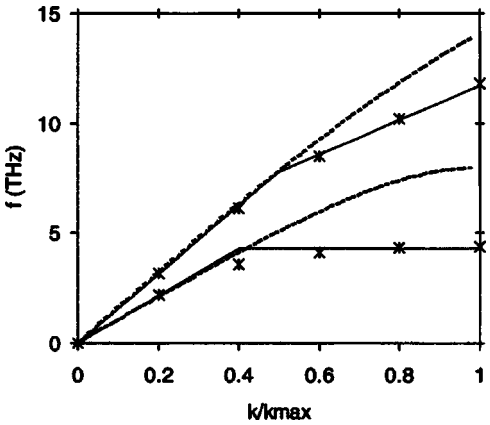

FIG. 2. Longitudinal- and transverse- (two degenerated curves) acoustic dispersion curves of bulk silicon in the [1,0,0] direction. Squares: experimental values. Continuous lines: linear fit of the experimental curves. Dashed lines: SW potential.

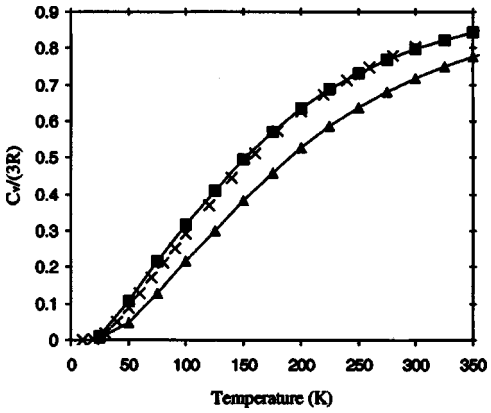

FIG. 3. The specific heat of silicon as a function of the temperature. Crosses: experimental data (see Ref. 37). Curve with triangle: Stillinger–Weber. Curve with squares: calculation with experimental dispersion curves fitted with linear curves.

izations and then six dispersion curves for each wave vector. The crystal is completely defined by the number of cells N_{a_1}, N_{a_2}, and N_{a_3} in the direction of each primitive vectors a_1, a_2, and a_3. The wave vectors describing the crystal vibrations are a linear combination of

$$K_{b_1} = 2n_{a_1}\pi/(N_{a_1}a_0), K_{b2} = 2n_{a2}\pi/(N_{a2}a_0) \tag{7a}$$

and

$$K_{b_3} = 2n_{a_3}\pi/(N_{a_3}a_0), \tag{7b}$$

where K_{bi} is in the direction of b_i, the reciprocal vector of a_i. The limiting values of n_{a_1}, n_{a_2}, and n_{a_3} are such that the wave vectors belong to the first Brillouin zone of the primitive cell. These limiting values also depend on the boundary conditions (periodic of fixed surfaces).[28] Actually, we have already shown that the type of boundary conditions does not significantly affect the value of the thermal conductivity.[29] Therefore, a first information about the geometry of the sample (shape, size, anisotropy, etc.) can be straightforwardly accounted for changing the values of N_{a_1}, N_{a_2}, and N_{a_3}.

For the sake of simplicity, the dispersion curves in the [1, 0, 0] direction are used for all the wave-vector directions where $K_{\max}$ is the largest wave vector of the first Brillouin zone. For convenience, the experimental curves were fitted with linear curves, as shown in Fig. 2. This linear fit is actually a good approximation, within less than 5% of the actual experimental values, except for the transverse mode around $k/k_{\max}=0.4$ where the maximum difference is about 15%.

The specific heat of silicon, calculated using the linear fit of the experimental dispersion curves (Fig. 3), is slightly higher than the experimental value at low temperatures (below 150 K), and both values are identical at higher temperatures. Hence, the use of this unique set of dispersion curves for all the wave-vector directions is a good approximation to recover the internal energy of silicon.

To calculate the thermal conductivity, it is necessary to know the relaxation time, which depends on the frequency of the vibration mode, the temperature, and the system size. For a crystal, assuming that the scattering mechanisms are not coupled, the expression representing the phenomenological variation of the relaxation time can be written as

$$\tau^{-1}(\omega) = \tau_U^{-1}(\omega) + \tau_{\mathrm{BC}}^{-1}(\omega) + \tau_d^{-1}(\omega), \tag{8}$$

with the relaxation time due to the umklapp processes (phonon-phonon interactions),[3,9–11] being

$$\tau_U^{-1}(\omega) = A\omega^{\chi}T^{\xi}\exp(-B/T). \tag{9}$$

The relaxation time due to phonon-defect interaction is written as[10]

$$\tau_d^{-1}(\omega) = D\omega^4. \tag{10}$$

Several expressions have been proposed for the relaxation time due to the presence of the system boundaries.[12,13,30] All of these are proportional to the relaxation time of the Casimir limit.[31] In this study, we consider the following expression:[15]

$$\tau_{\mathrm{BC}}^{-1}(\omega) = v(K,p)/[F^*L(K)], \tag{11}$$

where $L(K)$ is the distance that a phonon can travel between two boundary surfaces and F mainly depends on the surface roughness. All the parameters A, B, D, F, χ, and ξ have to be determined. In order to recover the experimental variations of the thermal conductivity of silicon, it is necessary to consider a different umklapp relaxation time for the longitudinal and transverse modes.[15] For nearly pure silicon, the parameter D mainly depends on the isotope concentration. Assuming that this concentration is constant, D should be a constant and has already been determined,[16]

$$D = 1.32 \times 10^{-45}\ \mathrm{s}^3.$$

Using Eqs. (5) and (8)–(11) and the experimental dispersion curves, all the parameters A_T, A_L, B_T, B_L, χ_T, ξ_T, χ_L, ξ_L, and F are fitted to match the variation of the experimental thermal conductivity of a bulk silicon crystal (Fig. 4) for which the characteristic length is equal to $L(k)=7.16\times10^{-3}$ m:[15]

$$A_T = 7 \times 10^{-13}, \quad B_T = B_L = 0, \quad A_L = 3 \times 10^{-21},$$

$$\chi_T = 1, \quad \xi_T = 4, \quad \chi_L = 2, \quad \xi_L = 1.5, \quad F = 0.55.$$

Assuming the same relaxation time for the acoustic and optical branches, the contribution of the optical vibration

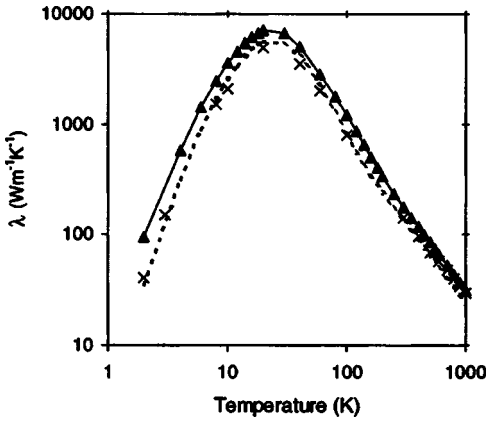

FIG. 4. Thermal conductivity of a silicon crystal $L=7.16\times10^{-3}$ m. Crosses: experimental values (see Ref. 15). Dashed line: results obtained with the experimental dispersion curves. Line with triangles: results obtained from the SW potential dispersion curves.

modes to the thermal conductivity increases with temperature, but the contribution remains at less than 3% of the thermal conductivity below 1000 K.

III. PREDICTION OF THERMAL CONDUCTIVITY OF SILICON NANOWIRES AND NANOFILMS

If the system is isotropic, and its size infinite, the sum in (5) becomes an integral, which is most conveniently reexpressed using a change of variables from wave vector K to angular velocity ω [through the dispersion curve and density of states $\mathcal{D}(\omega)$]. The result for λ becomes

$$\lambda = \frac{\hbar^2}{3k_bT^2V_{\mathrm{mol}}}\int_0^\infty v(\omega)^2\tau(\omega)\mathcal{D}(\omega)\frac{\omega^2 e^{\hbar\omega/k_bT}}{(e^{\hbar\omega/k_bT}-1)^b}d\omega. \quad (12)$$

Mingo[16] calculated the thermal conductivity of nanowires using this expression in which he replaced the bulk density of states and the group velocity by the same quantities as calculated from the set of dispersion curves of a nanowire. Using the Harisson[25] potential, the dispersion curves were obtained from the construction of the dynamical matrix of the system. For each wire diameter, Mingo found it necessary to fit the parameter F of the relaxation time [Eq. (11)] due to phonon-boundary diffusion in order to match the experimental results.

Calculating the phonon distribution function of a wire as a deviation from the distribution function of the bulk crystal, the thermal conductivity of a wire can be expressed as[12–14]

$$\lambda = \frac{\hbar^2}{3k_bT^2V_{\mathrm{mol}}}\int_0^\infty v(\omega)^2\tau(\omega)\mathcal{D}(\omega)\frac{\omega^2 e^{\hbar\omega/k_bT}}{(e^{\hbar\omega/k_bT}-1)^2} \times[1-G(\eta,\varepsilon)]d\omega, \quad (13)$$

where the function G depends on

(1) the wire section geometry,
(2) the ratio between the section characteristic length and the phonon mean free path η, and
(3) the roughness effect on the phonon-boundary scattering through the parameter ε. Asheghi *et al.*[7] have also proposed an equivalent expression for nanofilms.

To calculate the thermal conductivity of nanowires, the total relaxation time still includes the relaxation time due to the phonon-boundary diffusion, but for the nanofilms, Asheghi *et al.*[7] just considers the contribution of the umklapp process and phonon diffusion by defect. In each case, the parameter ε has to be fitted so that the model yields a good quantitative agreement with the experimental results.

In this section, we calculate the thermal conductivity of nanowires and nanofilms using Eqs. (5) and (8)–(11) in which all the parameters are those previously determined based on the experimental dispersion curves of bulk silicon. We assume that the phonon-boundary diffusion is the same in nanostructure as in the bulk crystal, so that the parameter F in Eq. (11) is constant whatever the size and geometry of the system. The only difference between the bulk crystal and the nanostructure lies in the sampling of the first Brillouin zone. Hence, it depends on the sample size and shape and becomes strongly nonisotropic for both films and wires. Moreover, the distance $L(K)$ depends on the wave-vector direction and is also nonisotropic for films and wires. This is the main advantage of our model since the anisotropy cannot be recovered using the angular velocity sampling [Eqs. (12) and (13)].

The thermal conductivity of silicon nanowires in the axial direction was measured by Li *et al.*[8] The authors estimated the length of their nanowires to be $L=2$ μm. For our analysis, we consider that the wire is built from the elementary crystal cell of silicon defined by the primitive vectors a_1, a_2, and a_3. Considering a_1 as the axial direction and the lattice parameter for silicon ($a_0=0.543$ nm), the number of cells in this direction is equal to 5209. The number of cells in the a_2 and a_3 directions is equal to 68, 115, 173, and 356 in order to get the same characteristic section lengths, d, in the plane perpendicular to the a_1 direction, as found in the experimental measurements, namely, 22, 37, 56, and 115 nm, respectively. The thermal conductivities of the wires in the axial direction are calculated using Eqs. (5) and (8)–(11) where $L(k)$ used in Eq. (11) is defined as

$$L(K) = d/\sin[\theta_{a_1}(K)] \quad (14a)$$

and

$$L(K) \leqslant L. \quad (14b)$$

Except for the smallest wire, our results are in good agreement with the experimental data (Fig. 5). The differences could not only be due to the experimental uncertainties in the measurements but also to the difference between the theoretical and experimental wire dimensions/geometries. In particular, the error, as compared to the experiment, is significantly smaller than the differences between the values obtained for different wire diameters. As such, this simple model can be used to reliably estimate the influence of diameter on the thermal conductivity. It seems that the bulk properties (dispersion curves and relaxation time) can be used to predict the thermal conductivity of nanowires down to 37 nm. For the smallest wire ($d=22$ nm), the value of the thermal conductivity at 300 K (13 W m^{-1} K^{-1}) is the same as the one calculated by Zou and Balandin[12] for a nanowire of

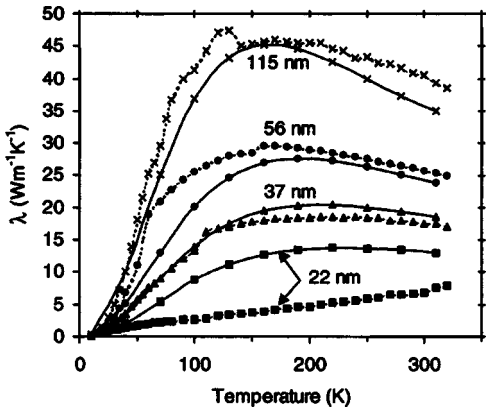

FIG. 5. Thermal conductivities of silicon nanowires vs temperature. Dashed lines: experimental data (see Ref. 8). Continuous lines: our prediction model. Each kind of symbol corresponds to a different section characteristic length.

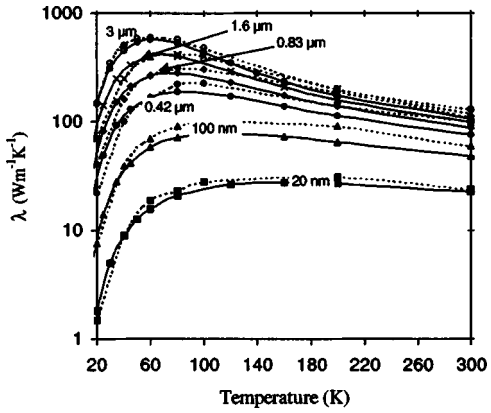

FIG. 6. Thermal conductivities of silicon nanofilms vs temperature. Dashed lines: experimental data (see Ref. 7). Continuous lines: our prediction model. Each kind of symbol corresponds to a different film thickness.

diameter $d=20$ nm. However, the variation of the experimental thermal conductivity of the smallest wire is completely different from those obtained for larger sections. This behavior, which is not predicted by our model, remains to be experimentally confirmed and theoretically understood. It could be argued that as the wire diameter decreases, the system approaches a one-dimensional (1D) behavior. It may have a transition between the three-dimensional (3D) and 1D behaviors for diameters between 20 and 30 nm. This transition can have a significant influence on the dispersion curves, the relaxation time, and the specific heat. As the wire diameter decreases, the influence of the surface defects (oxides and so on) can also be much more important and strongly modifies the vibration modes, as well as their diffusion, along the boundary surfaces. However, it remains puzzling that no such transition is observed in a film geometry, as shown below.

As for the wires, we consider that silicon nanofilms are built from elementary crystal cells of silicon. The in-plane directions are defined by vectors a_2 and a_3. The number of cells in the a_1 direction is equal to 90, 451, 1895, 3744, 7217, and 13 533 in order to have the same thickness, e, as the six films that have been characterized:[7,32,33] 20 nm, 100 nm, 420 nm, 830 nm, 1.6 μm, and 3 μm, respectively. The number of cells in the a_2 and a_3 directions should depend on the largest dimension of the film. For the two thinner films, this dimension is about 100—500 μm, but it is not known for the other films. Actually, the thermal conductivity varies when the number of cells in the plane direction increases, but there is a minimum number of cells after which the thermal conductivity remains constant. This minimum number of cells depends on the film thickness and temperature. We have used 2400 cells for the 20-nm film thickness, 720 cells for the case of 100- and 420-nm film thicknesses, and 300 cells for the larger film thickness. Regardless of the number of cells, since the larger dimension of the film is much greater than its thickness, the distance $L(K)$ used in Eq. (11) is equal to

$$L(K) = e/\sin[\theta_{a_1}(K)]. \tag{15}$$

The in-plane thermal conductivity of these films is calculated using Eqs. (5) and (8)–(11) and compared with the experimental values.[7,32,33] The agreement between the model and the experimental results is excellent for the two thinnest films (Fig. 6) for which the experimental uncertainty has been evaluated to be 5%.[33] For the remaining films, the model underestimates the thermal conductivity at high temperature. However, the qualitative variation of the thermal conductivity is quite well reproduced, and the absolute values remain within the range of the experimental uncertainty: 25% for the films of thickness 420 nm, 830 nm, and 1.6 μm (Ref. 7) and 12% for the 3-μm-thick film.[32]

In summary, we have shown in this section that a simple model based on the kinetic theory of phonons, using bulk properties as an input, can very reasonably account for experimental results concerning the thermal conductivities of various nanostructures. The geometry of the structure enters only through the sampling of the Brillouin zone. Other quantities entering the thermal conductivity are not affected by the geometry, at least for structures larger than 20–30 nm. This result is, in a sense, quite intuitive, since the bulk calculation does not involve any intermediate length scale at which a crossover to a different behavior should be expected.

IV. EVALUATION OF THE SW INTERATOMIC POTENTIAL FOR HEAT TRANSFER MD SIMULATION IN SILICON

As mentioned in the Introduction, MD is a powerful tool that permits to take into account the variation of the vibrational properties with the system size and the variation of the anharmonicity with the temperature level. Of course, the quality of the results directly depends on the quality of the interatomic potential used to calculate the interatomic forces. The aim of this section is to propose a methodology to evaluate the quality of an interatomic potential. Our approach is based on the observation of Sec. III, that even in nanostructures, thermal conductivity is essentially determined by bulk vibrational properties. Hence the general quality of an interatomic potential with respect to heat transfer modeling in nanostructures should be judged based on its ability to correctly reproduce those properties that are essential in heat transfer in the bulk.

TABLE I. Properties of bulk silicon.

		Elastic constants (Mbar)			Group velocities (m/s)			frequencies (THz)	
	Melting temperature (K)	C_{11}	C_{12}	C_{44}	LA at Γ	TA at Γ	LA at X	LA at X LO at X	TA at X
Expt.	1683[a]	1.7[b]	0.65[b]	0.81[b]	8480[c]	5860[c]	4240[d]	11.9[d]	4.35[d]
SW	1665–1691[a]	1.79[e]	0.72[e]	0.74[e]	8790[e]	5660[e]	5600[e]	13.9[e]	7.9[e]

[a]Reference 19.
[b]Reference 34.
[c]Reference 15.
[d]Reference 35.
[e]Data calculated using the code GULP (see Ref. 40).

In this section, silicon is still considered as the target material. Reviews of interatomic potentials for silicon have already been published[19,34] and it seems that no empirical model has been proposed since 1997. As explained by Bazant and Kaxiras,[34] almost all the empirical potentials for silicon fall into either the generic Stillinger–Weber[23] (SW) or Tersoff[24] forms. A simpler potential, for which the energy of the system is the sum of a two- and three-body harmonic terms, was earlier proposed by Harrison.[25] The SW model is considered in this section since the SW model has been used for the majority of dynamical heat transfer simulations, while the Harrison potential has just been used once,[16] and the Tersoff potential has never been used for such an application.

As phonon heat transfer is considered, the first essential ingredient of heat conductivity computations will be the dispersion curves. We first determine these curves for the SW potential and compare them with the experimental data, which are used as a reference.

Bulk silicon has a diamond structure, which is face-centered cubic and contains just two atoms in the primitive rhombohedral unit cell. Hence, the dispersion curves consist of one longitudinal-acoustic (LA) and two transverse-acoustic (TA) branches, as well as one longitudinal-optical (LO) and two transverse-optical (TO) branches, in each direction. For simplicity, only the dispersion curves in the [1, 0, 0] direction are compared with the experimental ones.[35,36] Using the conventional notation, the center of the Brillouin zone is the Γ point and the point on the limit of the Brillouin zone in the [1, 0, 0] direction is named X. In Fig. 2, only the acoustic branches are represented, and the two transverse modes are degenerated. The vibration frequencies at Γ and X are given in Table I, as the experimental data for the optical and acoustic branches for comparison.

The SW accurately reproduces the experimental acoustic dispersion curves as long as the wave vector is smaller than $0.4K_{max}$. Over this value, the SW model overestimates the vibrational frequencies and the group velocities for all modes. The vibration frequency of the TA mode at X point is largely overestimated. As the group velocities and the elastic behavior are related, the elastic constants of silicon obtained with the SW potential are compared to the experimental values (Table I). As expected, the SW potentials give a good estimate of the elastic constants.

Using Eq. (6), the specific heat of silicon is calculated as a function of the temperature based on the set of dispersion curves obtained from the SW potentials. The curve is plotted in Fig. 3 to be compared to the experimental specific heat.[37–39] At low-temperature, the lower-frequency vibrational modes constitute a large contribution to the internal energy. As the SW reproduces with a good accuracy the experimental dispersion curves in the limit of small wave vectors, it gives a good estimate of the specific heat at low temperature. At higher temperatures, overestimating the frequency range leads to an underestimation of the specific heat by between 25% and 10% for the SW potential when the temperature varies from 100 to 300 K.

The above considerations pertain to the frequency range of the vibrational modes, and to the propagation of the phonons through the crystal. However, the thermal conductivity also depends on phonon-phonon scattering, which is due to the anharmonic nature of the interactions. The quality of the anharmonic contribution of the interatomic potential can be evaluated through the variation of the atomic volume with the temperature, since thermal expansion is a purely anharmonic effect. As shown on Fig. 7, the variation of the density of Si obtained with the SW potential is very close to the experimental one. It can then be assumed that the phonon relaxation time due to the SW potential anharmonicity is the same as the value identified from the experimental values of the thermal conductivity (Sec. II). With this assumption, the

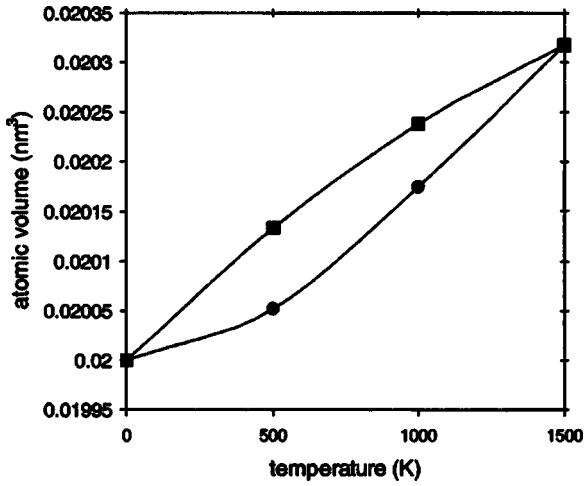

FIG. 7. Variation of the atomic volume as a function of the temperature (see Ref. 19). Circles: experimental values; squares: SW potential; the lines are guides for the eyes.

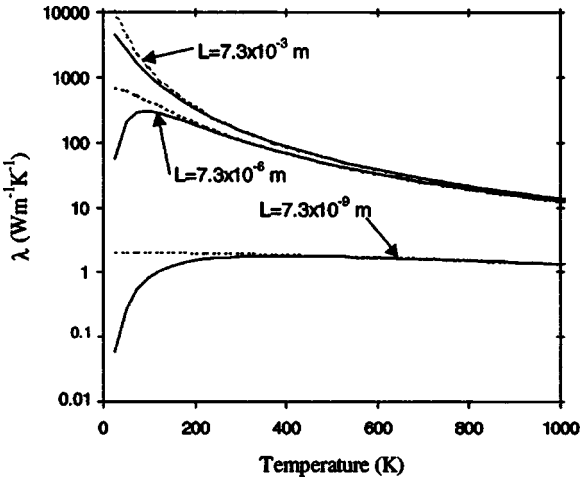

FIG. 8. Thermal conductivity calculated with the Planck distribution function (solid lines) and a constant specific heat (dashed lines) as a function of the temperature for three different characteristic lengths.

model developed in Sec. II can be used to predict the thermal conductivity that can be obtained from MD heat transfer simulations with the SW potential. These calculations show (Fig. 4) that the SW potential leads to an overestimate of the thermal conductivity by almost 100% at 2 K, 50% at 20 K, and 15% above 300 K.

In MD simulations, the phonon distribution function is constant whereas in the reality, phonons follow the Planck distribution function. To account for this effect, the thermal conductivity in our model can be calculated by replacing $C(K,p)$ with its limiting value at high temperature, k_b. This constant value corresponds to the classical description of the phonon distribution function as in MD simulations. The results are compared in Fig. 8 to the thermal conductivity previously calculated with the true value of the specific heat. As expected, the difference between the classical model and the model with the true distribution function for the phonons decreases when the temperature and the system size increase. For a system with a characteristic size of several nanometers, which is the typical system size that can be handled with MD, the difference between the constant and the Planck distribution function for phonons becomes negligible for temperatures larger than 300 K.

V. CONCLUSIONS

An analytical model has been used to study the heat transfer in silicon nanostructures based on the calculation of the contribution to the thermal conductivity of each vibration mode of a system. All the vibrational properties (dispersion curves and relaxation time) that are used in the model come from the bulk material. The size effect is taken into account through the sampling of the wave vectors and the distance a wave vector can travel in the structure between two boundaries. The model successfully predicts the thermal conductivity of silicon nanofilms for thicknesses down to 20 nm, and of silicon nanowires with diameters down to 37 nm. For thinner wires, the model appears to overestimate the thermal conductivity, but it is not clear whether it is due to an experimental artifact (larger uncertainties, stronger effect of the surface defects, etc.) or an inaccurate description of the heat transfer by the model due, for instance, to the deviation of the phonon dispersion with respect to the bulk.

The model has also been used to evaluate *a priori* the performance of the SW potential in MD simulations of heat transfer. Using the dispersion curves of the SW potential and the relaxation time identified from the experimental values of the thermal conductivity, the model show that the SW should overestimate thermal conductivities by an amount that varies between 100% and 15% as the temperature varies between 2 and 300 K. In practice, to predict the results that should be obtained with MD, the thermal conductivity has to be calculated assuming a constant distribution function for the phonons. Under these conditions, the model predicts that MD heat transfer simulations should lead to a much larger overestimation when the temperature is lower than 300 K. Above 300 K, MD heat transfer simulations should result in a slightly (typically less than 15%) overestimated conductivity.

ACKNOWLEDGMENT

The authors acknowledge partial funding from Région Rhône-Alpes through the "Thématiques prioritaires 2003-2005" program in material sciences. One of the authors (J.D.G.) would like to thank the Government of Western Australia for a Premier's Research Fellowship.

[1] C. J. Glassbrenner and G. A. Slack, Phys. Rev. **134**, A1058 (1964).
[2] G. A. Slack and C. Glassbrenner, Phys. Rev. **120**, 782 (1960).
[3] M. G. Holland, Phys. Rev. **134**, A471 (1964).
[4] K. E. Goodson, O. W. Kording, M. Rosler, and R. Zachai, J. Appl. Phys. **77**, 1385 (1995).
[5] D. Li, Y. Wu, R. Fan, P. Yang, and A. Majumdar, Appl. Phys. Lett. **83**, 3186 (2003).
[6] S. M. Lee and D. G. Cahill, J. Appl. Phys. **81**, 2590 (1997).
[7] M. Asheghi, M. N. Toulzelbaev, K. Goodson, Y. K. Leung, and S. S. Wong, ASME J. Heat Transfer **120**, 30 (1998).
[8] D. Li, Y. Wu, P. Kim, L. Shi, P. Yang, and A. Majumdar, Appl. Phys. Lett. **83**, 2934 (2003).
[9] J. Callaway, Phys. Rev. **113**, 1046 (1959).
[10] P. G. Klemens, Proc. Phys. Soc. London **48**, 1113 (1955).
[11] P. G. Klemens, *Solid State Physics*, edited by F. Steitz and D. Turnbull (Academic, NY, 1958).
[12] J. Zou and A. Balandin, J. Appl. Phys. **89**, 2932 (2001).
[13] X. Lu and J. H. Chu, J. Appl. Phys. **93**, 1219 (2003).
[14] S. G. Walkauskas, D. A. Broido, K. Kempa, and T. L. Reinecke, J. Appl. Phys. **85**, 2579 (1999).
[15] M. G. Holland, Phys. Rev. **132**, 2461 (1963).
[16] N. Mingo, Phys. Rev. B **68**, 113308 (2003).
[17] M. P. Allen and D. J. Tildesley, *Computer Simulation of Liquid* (Oxford University Press Inc., New York, 1987).
[18] D. Frenkel and S. Berend, *Understanding Molecular Simulation* (Academic, San Diego, CA, 1996).
[19] S. T. Cook and P. Clancy, Phys. Rev. B **47**, 7686 (1993).
[20] Y. H. Lee, R. Biswas, C. M. Soukoulis, C. Z. Wang, C. T. Chan, and K. M. Ho, Phys. Rev. B **43**, 6573 (1991).
[21] S. G. Volz and G. Chen, Phys. Rev. B **61**, 2651 (2000).
[22] P. K. Schelling, S. R. Phillpot, and P. Keblinski, Phys. Rev. B **65**, 144306 (2002).
[23] F. H. Stillinger and T. A. Weber, Phys. Rev. B **31**, 5262 (1985).
[24] J. Tersoff, Phys. Rev. B **39**, 5566 (1989).
[25] W. A. Harrison, *Electronic Structure and the Properties of Solids* (Dover, New York, 1989).
[26] R. Biswas and D. R. Hamann, Phys. Rev. Lett. **55**, 2001 (1985).

[27]E. R. Cooley, Phys. Rev. Lett. **60**, 2379 (1988).
[28]C. Kittel, *Introduction to Solid State Physics* (Wiley, New York, 1996), p. 673.
[29]P. Chantrenne and J. L. Barrat, ASME J. Heat Transfer **126**, 577 (2004).
[30]I. Rosenblum, J. Adler, and S. Brandon, Comput. Mater. Sci. **12**, 9 (1998).
[31]H. B. G. Casimir, Physica (Amsterdam) **5**, 595 (1938).
[32]M. Asheghi, K. Kurabayashi, R. Kasnavi, and K. E. Goodson, J. Appl. Phys. **91**, 5079 (2002).
[33]W. Liu and M. Asheghi, Appl. Phys. Lett. **84**, 3819 (2004).
[34]M. Z. Bazant and E. Kaxiras, Phys. Rev. B **56**, 8542 (1997).
[35]B. N. Brockhouse, Phys. Rev. Lett. **2**, 256 (1959).
[36]S. Wei and M. Y. Chou, Phys. Rev. B **50**, 2221 (1994).
[37]P. Flubacher, A. J. Leadbetter, and J. A. Morrison, Philos. Mag. **4**, 273 (1959).
[38]S. Weis, C. Li, and M. Y. Chou, Phys. Rev. B **50**, 14587 (1994).
[39]C. M. Rignanese, J. P. Michenaud, and X. Gonze, Phys. Rev. B **53**, 4488 (1996).
[40]J. D. Gale and A. L. Rohl, Mol. Simul. **29**, 291 (2003).